

Glass-formation and corrosion properties of Fe-Cr-Mo-C-B glassy ribbons with low Cr content.

Milad Madinehei^a, Pere Bruna^a, M. J. Duarte^b, Eloi Pineda^c, J. Klemm^b, F. U. Renner^d

^aDept. Física Aplicada, EPSC, Universitat Politècnica Catalunya - BarcelonaTech, Esteve Terradas 5, 08860 Castelldefels, Spain.

miladmadinehei@gmail.com / daniel.crespo@upc.edu

^b Department of Interface Chemistry and Surface Engineering, Max-Planck Institut für Eisenforschung GmbH, 40237 Düsseldorf, Germany

^cDept. Física i Enginyeria Nuclear, ESAB, Universitat Politècnica Catalunya - BarcelonaTech, Esteve Terradas 8, 08860 Castelldefels, Spain.

eloi.pineda@upc.edu

^d IMO/Hasselt University, Institute for Materials Research (IMO) Materials Physics Division, Wetenschapspark 1BE-3590 Diepenbeek, Belgium

*Corresponding author:

Milad Madinehei

miladmadinehei@gmail.com

Tel. (34) 934 134 156

Fax. (34) 934 137 007

Abstract

The effect of low amounts of Cr on glass forming ability and corrosion behavior of Fe_(65-x)Cr_xMo₁₄C₁₅B₆ ($x=0, 2, 4, 6, 8, 10$ at.%) ribbons have been studied. It was found that the reduced glass transition temperature (T_{rg}) do not change significantly with Cr content. The glass forming ability (GFA) of this system is evaluated by the γ_m , δ and ω parameters and the alloys containing 4 and 6 at.% were found to be the best glass formers in this system. The temperature interval of the supercooled liquid region (ΔT_x) changed with Cr and was enlarged from 35 K at $x=0$ to 50 K at $x=4$. Corrosion rates measured by immersion tests in H₂SO₄ decreased with an increase of chromium content in the alloys. The electrochemical measurements indicate that the alloys containing more than 4 at.% of Cr are spontaneously passivated with low current densities in 0.1 N H₂SO₄ whereas the alloys with Cr content < 4 at.% showed active behavior. In view of these results, the optimal amount of Cr addition in Fe-Mo-C-B amorphous steels is discussed.

Introduction

During recent years, metallic glasses have been a subject of great interest in the field of materials science and engineering because of their unique properties [1]. Amorphous Fe-based alloys including high-boron and carbon content in its composition (known as amorphous steels [2]) are regarded as having a high potential for industrial applications due to the high availability and low cost of the alloying elements [3]. These alloys have excellent magnetic and mechanical properties with fracture strengths as high as 4.4 GPa and plastic strain of 0.8% [4]. Recently their previous size limitation has been greatly overcome by adding a suitable amount of rare earth elements [2,3,5], thus increasing the production cost of the alloys, and many efforts have been carried out to understand the effect of various factors on the formation, thermal stability and properties of these alloys. In particular, the Fe-Cr-Mo-C-B system is widely studied due to its high glass-forming ability (GFA) and corrosion resistance in aggressive solutions [6–8]. The addition of Cr to amorphous steels benefits its corrosion resistance but it also affects the GFA and the mechanical response [9]. For instance, the ability to sustain plastic strain is negligible for Cr contents above 10 at.% [4]. However, all the corrosion studies of this system have been performed with compositions with a relatively large amount of Cr (from 15 at% in [6–8] and from 7.5 at% in [9]).

The high corrosion resistance of the Fe-Cr-Mo-C-B system is due to the formation of a chromium-rich passive film [10] and the amount of Cr will affect the corrosion resistance. The final passive film is essentially similar to the passive films formed on crystalline steels [11] but often lower Cr amounts are required for their formation [12]. Also the change of Cr content may influence the GFA of the alloy [9]. A particular composition of this system ($\text{Fe}_{50}\text{Cr}_{15}\text{Mo}_{14}\text{C}_{15}\text{B}_6$) has shown excellent properties [13]. In that paper the authors performed micro-electrochemical corrosion test on the as-quenched sample and after several heat treatments with partially or totally crystallized samples. They show how two different crystalline phases (rich in Mo and rich in Cr) appear and percolate throughout all the sample. The effect of a corrosion agent is to dissolve the Mo-rich phase and the resulting mesoporous Cr-rich phase is very stable and may be useful for different applications.

The aim of the present paper is to assess the minimum amount of Cr needed to develop a corrosion protective film without losing the high thermal stability and GFA. Thus, we study the effect of small additions of Cr ($x=0, 2, 4, 6, 8, 10$ at.%) in the $\text{Fe}_{(65-x)}\text{Cr}_x\text{Mo}_{14}\text{C}_{15}\text{B}_6$ system. To our knowledge, compositions with $x=2, 8$ and 10 have been never reported before in the literature. The corrosion study will be restricted here to the behavior in H_2SO_4 solutions.

1. Materials and methods

Master alloys were prepared by arc melting the mixture of constituent elements under a Ti-gettered Ar atmosphere. The purity of the elements were 99.95% for Fe, 99.95% for Cr, 99.95% for Mo, 99.98% for C and 99% for B. From the master alloys, amorphous samples were prepared in ribbon shape in an Ar atmosphere with purity of 99.9%. The thickness of the ribbons was ~ 40 μm and the width between 1 and 2 mm. The amorphicity of the samples was verified by x-ray diffraction (XRD) using Cu-K α radiation in a Bruker AXS instrument, set up in 2θ angle with a step size of 0.05° from 20 to 110° . Ribbons with 15 at% Cr has also been produced in order to have a reference with high Cr content.

In order to thermally characterize the ribbons, high temperature DSC (HT-DSC) was performed at a heating rate of 20 K/min. The glass transition temperature (T_g), the onset temperature of the first crystallization event (T_x), the solidus temperature (T_m) and the liquidus temperature (T_l) were determined using a NETZCH DSC 404F3 DSC under protection controlled atmosphere of N $_2$ gas (flow rate: 50 mL/min).

Corrosion resistance evaluations were carried out by mass loss and electrochemical measurements. Prior to any electrochemical and mass loss test, all samples were ion milled for 5 min to remove the surface oxide layer in a Gatan Co., Model 682 PECS with Ar ions at 5 KeV and tilting angle of 70° . Electrochemical measurements were done using a three electrode cell with an Ag/AgCl reference electrode and carbon counter electrode. The working electrode was exposed to an area of 1 cm^2 . Anodic polarization curves were measured potentiodynamically in the respective solution at room temperature with a sweep rate of 2 mV s^{-1} , after immersion of the specimens for 15 min, when the open-circuit potentials became almost steady. In order to have a high reliability of the results, all electrochemical measurements were repeated five times. After polarization in breaking down potential for 1000 s in H $_2$ SO $_4$ electrolyte, SEM images were taken from the surface of the specimens. In order to remove the corrosion products from the surface, prior to SEM investigation, the specimens were washed in distilled water and dried. The corrosion rates were estimated from the weight loss after immersion in 6N H $_2$ SO $_4$ solution open to air at 298 K for 168 h. Electrolyte used was prepared from reagent grade chemical and distilled water. After the immersion test, the specimens were washed in distilled water, dried, and subjected to weight loss measurement.

2. Results and discussion

Fig. 1 collects the X-ray diffraction patterns of the melt-spun alloys. The XRD patterns show only one broad peak in the 2θ range between 40 and 50° and no diffraction peak corresponding to a crystalline phase is seen for all the alloys as the figure illustrates. All samples are thus in a fully amorphous state. The respective DSC scans (shown in Fig. 2) revealing that multistage

crystallization occurs in all the samples. The obtained values of T_g , T_x , T_m and T_l are reported in Table 1.

The characteristic temperatures for $x=0, 4$ and 6 at.% alloys are in agreement with those found in the literature [4]. Using these transformation temperatures several parameters generally employed to indicate the thermal stability and GFA of amorphous alloys can be calculated [14]: the supercooled liquid range $\Delta T_x = T_x - T_g$, the reduced glass transition temperature $T_{rg} = T_g / T_l$, $\gamma = T_x / (T_g + T_l)$, $\gamma_m = 2T_x - T_g / T_l$, $\delta = T_x / (T_l - T_g)$ and $\omega = T_g / T_x - (2T_g / (T_g + T_l))$. A wider ΔT_x region suggests more resistance to crystallization [15]. The higher the T_{rg} , the smaller the supercooled liquid region the system has to bypass without crystallizing during the quenching and, hence, the smaller the critical cooling rate needed for glass formation [16]. For multicomponent metallic glasses the measure of γ has been reported to be more accurate than T_{rg} [17]. To improve this γ parameter, Du et al. had also considered ΔT_x in addition of T_x and T_l and proposed γ_m [18]. Considering the rate of nucleation and combining with the viscosity of the melt, Chen et al. [19] proposed δ to determine the GFA. Finally, for bulk samples it has been shown that the ω parameter exhibits the strongest interrelationship with the critical radius of the bulk sample when compared to other criteria reported so far [20]. All these parameters are summarized in Table 1. Ideal values for highest GFA are defined in the limit where T_g , T_x and T_l are equal to each other [14].

The ΔT_x value for the alloys studied in this work is in the range from 35 to 48 K. The largest ΔT_x value was obtained for $x=4$ at.% alloy which reveals the highest thermal stability. It was found that T_{rg} was almost independent of the chromium content and kept at constant value of about 0.55 in the composition range between 0-10 at.% Cr for the present alloys. Although the calculated parameters for Cr content between 4 and 8 at.% are remarkably close to each other, it was found that the different criteria defining the highest GFA correspond to the alloys either with 4 or 6 at.% Cr. The alloy with 6 at.% of Cr has the highest values of γ and δ . On the other hand, according to the values of γ_m and ω the alloy with 4 at.% of Cr has the best glass-forming ability. This fact can be explained because the supercooled liquid region is considered in these last two GFA criteria. According to the melting behavior, no single melting peak is observed in the DSC measurements (Fig. 2) of these six alloys indicating that they are not at eutectic points. The shortest melting interval ($T_l - T_m$) corresponds to the alloy with 6 at.% of Cr being therefore the closest alloy to the eutectic point. By combining these results, it can be said from the present study that considering γ and δ criteria, the best glass forming alloy is the one closest to a eutectic composition. It can be also noticed that the alloy with 10 at.% of Cr has the largest melting interval while does not have the poorest GFA among these six alloys.

To evaluate the corrosion behavior, immersion tests in 6N H₂SO₄ solution for 168 hours at 295 K open to air have been performed. Fig. 3 shows the respective corrosion rates of all the ribbons. The glassy ribbons containing 2 at.% and 4 at.% of Cr had already low corrosion rates of $\sim 10^{-1}$ mm/year in H₂SO₄ solution at room temperature, this is one order of magnitude lower than the Cr-free alloy. For alloys containing 6 or more at.% of Cr the corrosion rate dropped substantially. Increasing the Cr content further does not produce drastic changes in the dissolution rate obtaining values in the range between 2×10^{-2} and 5×10^{-2} mm/year. For comparison, the high Cr alloy with $x=15$ at.% [13], has been also tested showing a corrosion rate of the same order of magnitude than those obtained for $x=6$.

In addition to the immersion tests faster potential sweep measurements have been performed to gain additional information on the initial potential-dependent corrosion behavior. The electrochemical measurements in 0.1N H₂SO₄ solution, shown in Figure 4, indicate that samples without and with 2 at.% of Cr show a rather active-like behavior in H₂SO₄ compared to samples containing higher amounts of Cr. The respective steep rise in current corresponds to the known transpassive Mo dissolution observed for Mo-based alloys. For more than 4 at.% Cr the samples exhibit similar polarization behavior to each other and are spontaneously passivated with a relatively wide passivation region and low passive current densities. In addition, it is also seen that the alloys containing a larger amount of chromium show lower passive current densities but almost the same breakdown potential. Such a dependence of the passive current on the Cr content was earlier reported by Kirchheim for crystalline Fe-Cr alloys [11].

The sample containing 4 at.% Cr shows a very pronounced transition peak at about 0.2 V which indicates the transformation of an existing native oxide layer (with an oxide reflecting the bulk composition) towards a Cr-rich passive film. The passive current observed during the potential sweep is for this sample also considerably higher than for the samples with even higher Cr content. For all alloys containing 4 at.% of Cr and more, a current plateau or further peak is visible which extends from about 0.8V up to a steep rise in current at about 1.5 V vs. Ag/AgCl. This strong electrochemical current at about 1.5 V has its onset approximately at the usually observed transpassive Cr dissolution of pure Cr, while Fe-based alloys are typically shifted to lower values (showing a co-dissolution effect). While the potentiodynamic scans are thus instructive for the formation of the initial passive film at lower potentials, a more exact description of the breakdown behavior requires at this point more information of the specific surface states or on gas evolution reactions, which might be also involved but cannot be distinguished from current measurements alone. This is at that point beyond the scope of the presented initial screening experiments and will be addressed in following work. From the

results obtained it can be said that more than 4 at.% of Cr should be included in the Fe-Cr-Mo-C-B system to form a passive film leading to a reasonably high corrosion resistance.

Fig. 5 shows SEM micrographs of the surface of $x=0, 4$ and 8 alloys after the polarization tests in $0.1N H_2SO_4$ for 1000 s. These images show that as Cr increases in the composition, the corroded surfaces are less damaged. In Fig. 5 (a) the surface of the alloy with $x=0$ is completely damaged related to an increase of the corrosion products. In Fig. 5 (b) several round-shaped micrometer-sized pits-like regions are visible for the alloy with $x=4$ whereas in Fig. 5 (c) still some pores or pits are observed on the surface with $x=8$. However, its surface is less damaged in comparison to the sample without Cr and 4 at.% of Cr. Moreover, the pores observed in the alloy with 8 at.% resemble to selective dissolution of Cr-depleted regions probably dependent of inhomogeneities in the composition on the surface [13].

It is known that Cr is one of the most effective alloying elements providing a high passivating ability for the Fe-Cr-metalloid glassy alloys [21,22]. Corrosion resistance in metallic glasses is enhanced by producing spontaneous passivation related to the formation of a thin homogeneous film of Cr oxide. In general, compared to stainless steels which require at minimum 13 at.% Cr, this glassy alloy system needs only $4-6$ at.% of Cr for achieving stable passivity. For a better understanding of the corrosion mechanism and the effect of chromium addition on the corrosion behavior of $Fe_{(65-x)}Cr_xMo_{14}C_{15}B_6$ ($x=0, 2, 4, 6, 8, 10$ at.%) alloys, X-ray photoelectron spectroscopy (XPS) after polarization and immersion tests and extended X-ray absorption fine structure (EXAFS) studies are currently being performed. The results will be published elsewhere.

3. Conclusions

The glass forming ability and corrosion resistance of an amorphous steel in the low Cr concentration range (from 0 to 10 at%) has been studied in order to determine the optimal amount of Cr needed to obtain good corrosion properties while maintaining a high GFA. ΔT_x values are found in the range from 35 to 48 K for $Fe_{(65-x)}Cr_xMo_{14}C_{15}B_6$ ($x=0, 2, 4, 6, 8, 10$ at.%) ribbons and, in particular, partial replacement of 4 at.% Fe by Cr reveals the widest ΔT_x , therefore the highest thermal stability. According to the assessment of different GFA criteria, the best glass forming ability is observed for the samples with 4 and 6% of Cr although a high GFA is expected in all the series.

From electrochemical measurements and immersion tests, the substitution of $4-6$ at.% Fe by Cr is found to be effective in enhancing the corrosion resistance for this Fe-based amorphous system. The polarization curves performed in $0.1N H_2SO_4$ showed that passivation is already

observed for $x=4$ at.% and only a slight improvement (more noble values) of the breakdown potential are obtained for higher Cr-contents. The immersion tests in 6N H₂SO₄ showed high corrosion resistance for all the compositions from $x=6$ to 15 at.%. These results show that Fe-Cr-Mo-C-B alloys with large casting sizes, high thermal stability and good corrosion resistance in acidic environments can be obtained with Cr additions near 5 at.%, more Cr decreases the GFA and do not improve significantly the corrosion behavior.

Further work includes the study of the corrosion behavior of the alloys $x=4$ and $x=6$ with different degrees of crystallized fraction in order to see the formation of the mesoporous Cr-rich phase that is observed in the $x=15$ phase [13]. If this structure also appears in low Cr compositions that can be produced as rods, the range of applications of these kinds of materials will be considerably expanded.

Acknowledgements

Work funded by CICYT grant MAT2010-14907 and Generalitat de Catalunya grants 2009SGR1225 and 2009SGR1251. M. Madinehei acknowledges financial support from Generalitat de Catalunya grant FI-DGR.

References

- [1] J.R. Scully, A. Gebert, J.H. Payer, Corrosion and related mechanical properties of bulk metallic glasses, *J. Mater. Res.* 22 (2011) 302–313.
- [2] A. Bouchareb, B. Bendjemil, R. Piccin, M. Baricco, Influence of Rare-Earth Substitution for Iron in FeCrMoCB Bulk Metallic Glasses, *Chinese Phys. Lett.* 27 (2010) 076103.
- [3] M. Iqbal, J.I. Akhter, H.F. Zhang, Z.Q. Hu, Synthesis and characterization of bulk amorphous steels, *J. Non. Cryst. Solids.* 354 (2008) 3284–3290.
- [4] X.J. Gu, S.J. Poon, G.J. Shiflet, Mechanical properties of iron-based bulk metallic glasses, *J. Mater. Res.* 22 (2007) 344–351.
- [5] Q. Chen, D. Zhang, J. Shen, H. Fan, J. Sun, Effect of yttrium on the glass-forming ability of Fe–Cr–Mo–C–B bulk amorphous alloys, *J. Alloys Compd.* 427 (2007) 190–193.
- [6] P.F. Gostin, A. Gebert, L. Schultz, Comparison of the corrosion of bulk amorphous steel with conventional steel, *Corros. Sci.* 52 (2010) 273–281.
- [7] F. Gostin, U. Siegel, C. Mickel, S. Baunack, A. Gebert, L. Schultz, Corrosion behavior of the bulk glassy (Fe_{44.3}Cr₅Co₅Mo_{12.8}Mn_{11.2}C_{15.8}B_{5.9})_{98.5}Y_{1.5} alloy, *J. Mater. Res.* 24 (2011) 1471–1479.

- [8] Q.J. Chen, L.L. Hu, X.L. Zhou, X.Z. Hua, Y.J. Yang, Effect of Corrosive Medium on the Corrosion Resistance of FeCrMoCB Amorphous Alloy Coating, *Adv. Mater. Res.* 291 (2011) 65–71.
- [9] S. Pang, T. Zhang, K. Asami, A. Inoue, Effects of chromium on the glass formation and corrosion behavior of bulk glassy Fe-Cr-Mo-CB alloys, *Mater. Trans.* (2002).
- [10] S.J. Pang, T. Zhang, K. Asami, A. Inoue, Bulk glassy Fe–Cr–Mo–C–B alloys with high corrosion resistance, *Corros. Sci.* 44 (2002) 1847–1856.
- [11] R. Kirchheim, B. Heine, H. Fischmeister, S. Hofmann, H. Knote, U. Stolz, The passivity of iron-chromium alloys, *Corros. Sci.* 29 (1989) 899–917.
- [12] K. Hashimoto, What we have learned from studies on chemical properties of amorphous alloys?, *Appl. Surf. Sci.* 257 (2011) 8141–8150.
- [13] M.J. Duarte, J. Klemm, S.O. Klemm, K.J.J. Mayrhofer, M. Stratmann, S. Borodin, et al., Element-resolved corrosion analysis of stainless-type glass-forming steels., *Science*. 341 (2013) 372–6.
- [14] C. Suryanarayana, A. Inoue, *Bulk metallic glasses*, Taylor & Francis US, 2011.
- [15] L. Ma, A. Inoue, On glass-forming ability of Fe-based amorphous alloys, *Mater. Lett.* 38 (1999) 58–61.
- [16] Z.P. Lu, Y. Li, S.C. Ng, Reduced glass transition temperature and glass forming ability of bulk glass forming alloys, *J. Non. Cryst. Solids.* 270 (2000) 103–114.
- [17] Z.P. Lu, C.T. Liu, A new glass-forming ability criterion for bulk metallic glasses, *Acta Mater.* 50 (2002) 3501–3512.
- [18] X.H. Du, J.C. Huang, C.T. Liu, Z.P. Lu, New criterion of glass forming ability for bulk metallic glasses, *J. Appl. Phys.* 101 (2007) 086108.
- [19] Q. Chen, J. Shen, D. Zhang, H. Fan, J. Sun, D.G. McCartney, A new criterion for evaluating the glass-forming ability of bulk metallic glasses, *Mater. Sci. Eng. A.* 433 (2006) 155–160.
- [20] Z. Long, H. Wei, Y. Ding, P. Zhang, G. Xie, A. Inoue, A new criterion for predicting the glass-forming ability of bulk metallic glasses, *J. Alloys Compd.* 475 (2009) 207–219.
- [21] S.L. Wang, S. Yi, The corrosion behaviors of Fe-based bulk metallic glasses in a sulfuric solution at 70°C, *Intermetallics.* 18 (2010) 1950–1953.
- [22] S.. Pang, T. Zhang, K. Asami, A. Inoue, Synthesis of Fe–Cr–Mo–C–B–P bulk metallic glasses with high corrosion resistance, *Acta Mater.* 50 (2002) 489–497.

Table captions

Table 1. Characteristic temperatures and GFA parameters of the $\text{Fe}_{(65-x)}\text{Cr}_x\text{Mo}_{14}\text{C}_{15}\text{B}_6$ alloys.

Figure captions

Figure 1. X-ray diffraction pattern of the $\text{Fe}_{(65-x)}\text{Cr}_x\text{Mo}_{14}\text{C}_{15}\text{B}_6$ amorphous melt-spun ribbons.

Figure 2. DSC curves of $\text{Fe}_{(65-x)}\text{Cr}_x\text{Mo}_{14}\text{C}_{15}\text{B}_6$ alloys at a heating rate of 20 K/min.

Figure 3. Corrosion rates of the $\text{Fe}_{(65-x)}\text{Cr}_x\text{Mo}_{14}\text{C}_{15}\text{B}_6$ amorphous alloys in H_2SO_4 plotted versus chromium contents.

Figure 4. Linear polarization sweeps for $\text{Fe}_{(65-x)}\text{Cr}_x\text{Mo}_{14}\text{C}_{15}\text{B}_6$ ($x=0, 2, 4, 6, 8, 10$ at.%) in H_2SO_4 solution obtained at 2 mV/s.

Fig. 5. SEM micrographs of the surface of polarized $\text{Fe}_{(65-x)}\text{Cr}_x\text{Mo}_{14}\text{C}_{15}\text{B}_6$ ($x=0, 4, 8$ at.%) ribbons for 1000 s in 0.1N H_2SO_4 at breaking down potentials.

Table1. Values of the characteristic temperatures and GFA parameters of the $Fe_{65-x}Cr_xMo_{14}C_{15}B_6$ alloys

Addition of Cr element	T_g	T_x	T_m	T_l	ΔT_x	T_{rg}	γ	γ_m	δ	ω
x=0	515	550	1077	1145	35	0.555	0.373	0.605	1.306	0.243
x=2	519	562	1083	1150	43	0.556	0.376	0.617	1.323	0.233
x=4	526	576	1091	1160	50	0.557	0.380	0.627	1.339	0.225
x=6	531	579	1097	1163	48	0.560	0.381	0.626	1.348	0.226
x=8	532	580	1103	1170	48	0.558	0.379	0.624	1.336	0.227
x=10	536	581	1105	1183	45	0.556	0.377	0.617	1.319	0.232

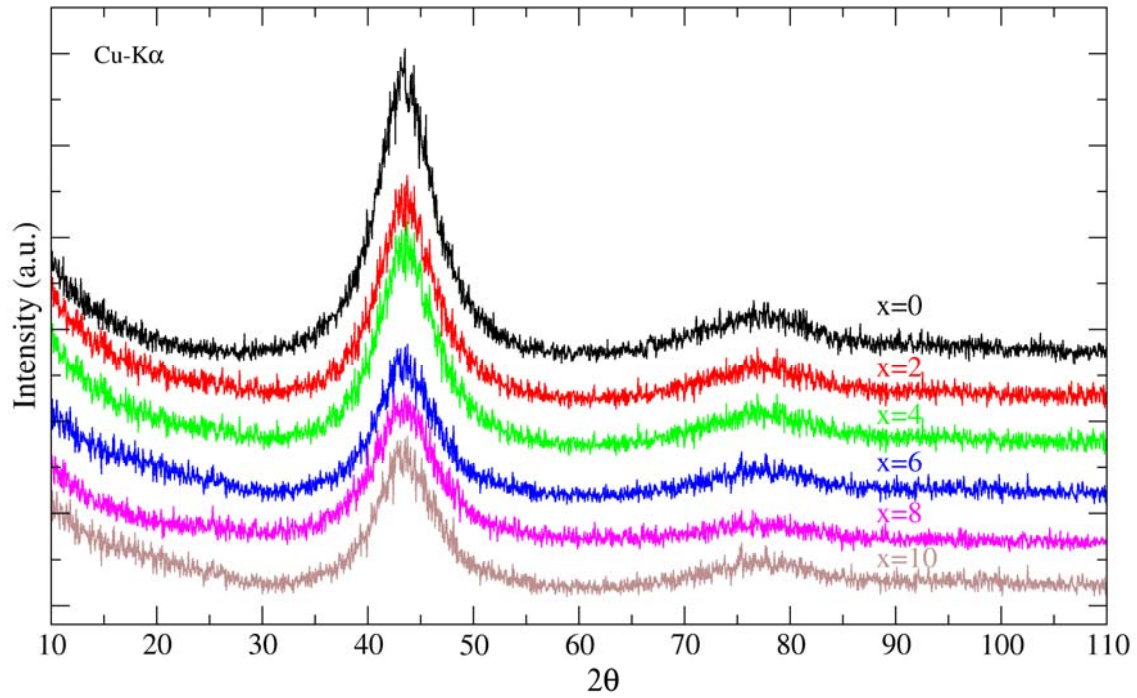


Fig. 1. X-ray diffraction pattern of the $Fe_{65-x}Cr_xMo_{14}C_{15}B_6$ amorphous melt-spun ribbons

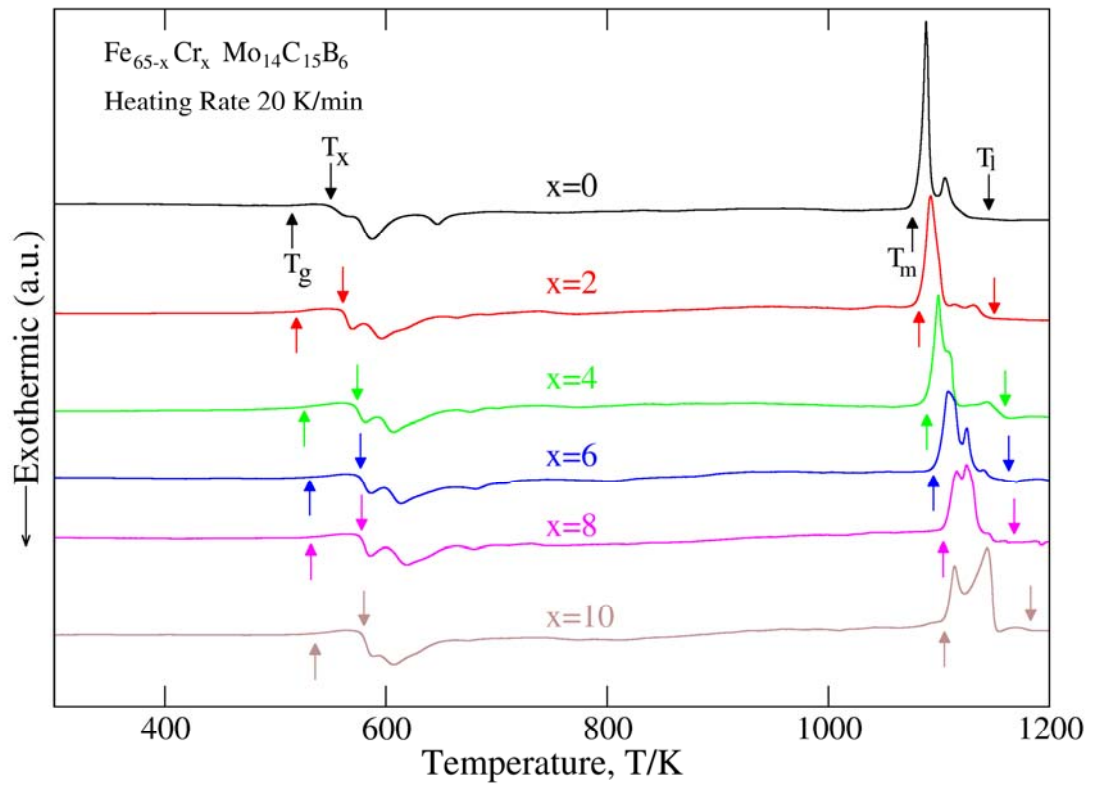


Fig. 2. DSC curves of $Fe_{65-x}Cr_xMo_{14}C_{15}B_6$ alloys at a heating rate of 20 K/min.

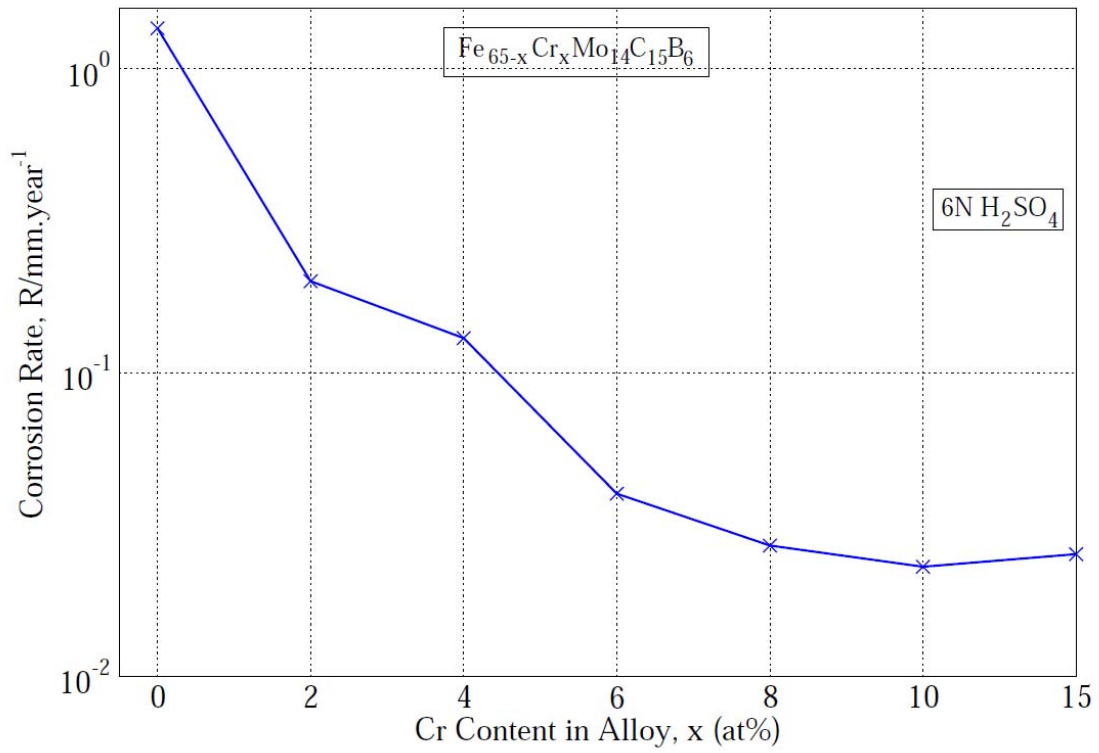


Fig. 3. Corrosion rates of the $Fe_{65-x}Cr_xMo_{14}C_{15}B_6$ amorphous alloys in H_2SO_4 plotted versus chromium contents.

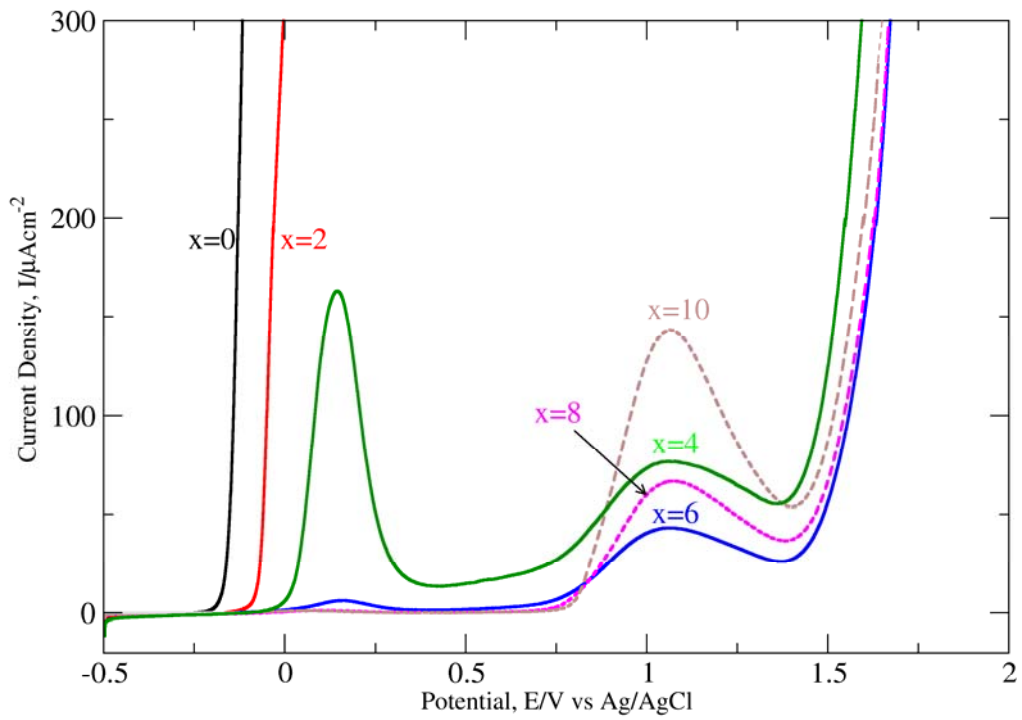


Fig.4. Linear polarization sweeps for $Fe_{65-x}Cr_xMo_{14}C_{15}B_6$ ($x = 0, 2, 4, 6, 8, 10$ at.%) in H_2SO_4 solution

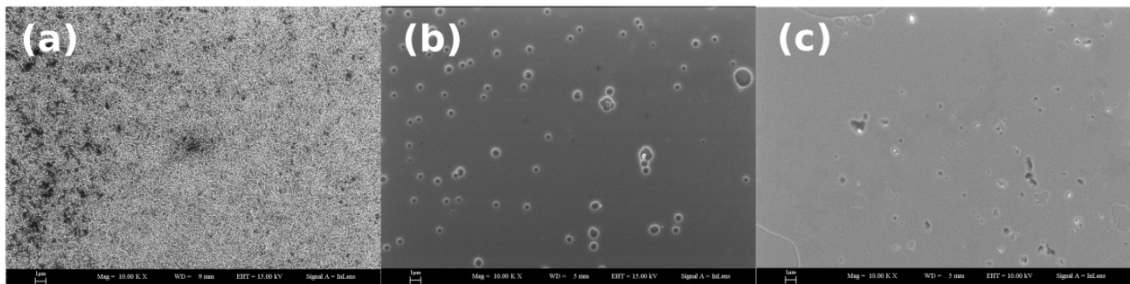


Fig. 5. SEM micrographs of the surface of polarized $Fe_{65-x}Cr_xMo_{14}C_{15}B_6$ ($x = 0, 4, 8$ at.%) ribbons for 1000s in 0.1N H_2SO_4 at breaking down potentials

